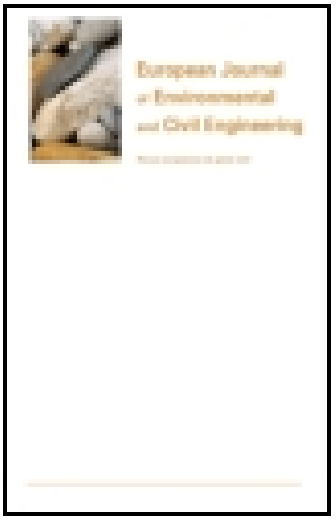

European Journal of Environmental and Civil Engineering

Publication details, including instructions for authors and subscription information:
http://www.tandfonline.com/loi/tece20

# Analysis of slope movement initiation induced by rainfall using the Elastoplastic Barcelona Basic Model

M. Jamei[a], H. Guiras[a] & S. Olivella[b]

[a] Civil Engineering Laboratory, National Engineering School of Tunis, Tunis El Manar University, Tunis, Tunisia

[b] Department of Geotechnical Engineering and Geosciences, Universitat Politecnica de Catalunya, Barcelona, Spain

Published online: 28 Jan 2015.

*European Journal of Environmental and Civil Engineering*, 2015
http://dx.doi.org/10.1080/19648189.2014.996670



# Analysis of slope movement initiation induced by rainfall using the Elastoplastic Barcelona Basic Model

M. Jamei[a]*, H. Guiras[a] and S. Olivella[b]

[a]*Civil Engineering Laboratory, National Engineering School of Tunis, Tunis El Manar University, Tunis, Tunisia;* [b]*Department of Geotechnical Engineering and Geosciences, Universitat Politecnica de Catalunya, Barcelona, Spain*

(*Received 4 March 2014; accepted 24 November 2014*)

In some arid and semi-arid regions, different types of infrastructure assets suffer from degradation of the roads, the embankment failures, erosion due to cyclic hydraulic actions and the effects of rainfall infiltration on slopes. Typical cases, such as the national roads in the north-west of Tunisia (Béja city) have been affected dramatically. Recent landslide is manifested in this region, especially in a plastic clay soil. Stability problems are caused by soil saturation and the presence of abundant cracks which are developed after a long dry summer. In fact, due to geotechnical problems, the annual loss due to the damage is estimated at $1 million in Béja area (30 $km^2$). The effect of rainfall infiltration into the unsaturated clay during wet seasons characterised by either long duration low intensity rain or short duration high intensity rain have been analysed. The elastoplastic Barcelona Basic Model (BBM) has been used and soil movements leading to slope failure were calculated according to the unsaturated state evolution. The effects of cyclic hydraulic paths on the yield function have also been investigated. The yield function evolution depends on the cohesion and the apparent consolidation stress variations. The numerical calculations were evaluated against the field measurement displacements.

**Keywords:** slope; movements; unsaturated clay; suction; wetting; drying

**Mots-clés**: talus; déplacements; argile non saturée; succion; humidification; drainage

## 1. Introduction

Slope analysis is an old geotechnical problem. Its treatment was often investigated with different approaches (equilibrium limit analyses as a conventional method but widely used; Alonso & Lioret, 1983; Chapuis, Chenaf, Bussière, Aubertin, & Crespo, 2001, gravity loading method and elastoplastic methods, as an example of the c-phi reduction method). In general, these approaches consider hydraulic and mechanical coupling problems via the groundwater level or depth data. As it was mentioned by Borja and White (2010), the most common approach of these methods is to uncouple the fluid flow and slope-stability problem, and treat them in a sequential fashion instead. Through the limit equilibrium approach, the most common treatment of slope-stability assumes that the unsaturated zone characteristics are constant and do not depend on water content evolution. However, many shallow landslides are really induced by water content evolution, particularly in the unsaturated zone (Rees & Thomas, 1994), which depend on the intensity and duration of the rainfall. Then, the rate of damage and the ground

*Corresponding author. Email: mehjamei@yahoo.fr

deformation evolution when the slope failure occurs are completely related to changes of soil suction (or water content). Numerous examples of world wide, large-scale slope failures triggered by the rainfall were reported by Borja and White (2010). The authors mentioned also the high costs and the number of deaths, associated to these kinds of landslides. As mentioned by Au (1998), different slopes in Hong Kong collapsed catastrophically without prior signs of warning. According to this Author, in Hong Kong, except for very limited number of failures caused by unscrupulous cutting, slope failures are mainly rain-induced. Dai, Lee, and Sijing (1999) gave the same conclusion. Another example is the La Conchita landslide, which occurred without warning on 11 January 2005, in south of California (Borja & White, 2010). Recently, few investigations have been engaged using field instrumentation, to study rainfall infiltration (Gong, Bao, NG, Fredlund, & Zhan, 2003; Orense Rolando, Suguru Shlmoma, Kengo Maeda, & Ikuo Towhata, 2004; Zhang, Zhang, & Tang, 2005). Gong et al. (2003) instrumented an 11 m high cut slope in a typical medium-plastic expansive clay soil. It was shown that the initial high soil suction induced a high increase in water content by wetting and led to horizontal stresses and soil deformation at the top right after the beginning of the rainfall (1–2 days) and the failure was shallow. Concerning the effect of the humidification process by the action of the rainfall, Orense Rolando et al. (2004), Lim, Rahardjo, Chang, and Fredlund (1996) achieved the same conclusion. Firstly, the continuous rainwater infiltration alone does not cause slope failure. Secondly, slope instability occurs only when the pore water pressure increases and the water table is allowed to rise. It was also shown that a local slope instability zone is developed against the water table rise (Smith, 2003). The explanation given by the authors is allocated to a reduction of the effective stress by the pore pressure increase and consequently the reduction of shear stress. Their interpretation is based on the effective stresses principle assumption. In the unsaturated soil, the principle was already revised Tamagnini and Pastor (2004). It is now known that the independent variables principle is also a convenient framework to explain the unsaturated soil behaviour (Josa, Alonso, & Gens, 1990). The variables are the total suction ($u_a - u_w$) and the total net stress ($\sigma - u_a$).

It is well known that to solve a multiphase problem it is needed to define a stress for each phase, to write the constitutive relations of each phase. However, to our knowledge, for unsaturated soils, it is not still possible to reach the measure of the effective stress. In laboratory, under the shear path, the suction is controlled by applying separately the water pressure and the air pressure (translation axis method). To deduce the value of the effective stress is not possible, without an additional assumption on the effective stress definition, as for example the Bishop's effective stress. Besides, it is useful to mention that some authors as Laloui and Nuth (2009) proposed a generalized effective stress concept versus Bishop's effective stress. These authors discussed the limitation of the last definition, in the elastoplastic framework of unsaturated soil. Also, the effective stress calculation requires a given definition. In this sense, Laloui and Nuth (2009) proposed to consider the effective stress as function of net stress and either suction and saturation degree.

Consequently, we are not yet, really able to characterize the effective parameters to obtain the constitutive relation for the phase skeleton. In the opposite, the total net stress and the suction can be measured and controlled separately. In this sense, the modeling of unsaturated soils can be properly conducted with the net total stress and suction as "proper" constitutive variables. This modeling way can be more supported by the obtained numerical results comparing to the field measured results.

In the other optic, to study the landslide initiation and propagation, most of the works related to this problem have been conducted within a framework of bifurcation

theory, using elastoplastic approach (see for instance Fernandez Merodo et al., 2004; Herrores et al., 2002; Pastor et al., 2013; Pastor et al., 2004) or the second-order work (Buscarnera & Prisco, 2012; Nicot, Darve, & Dat Vu Khoa, 2007). The use of elastoplastic approach by Frenadez et al. (2004) with a generalised plasticity provides a unified formulation for both initiation and propagation phases. It can also represent the mechanical collapse of material under saturation evolution. However, the use of second-order work in unsaturated soils is more recently and a few results are presented in literature (Buscarnera & Prisco, 2012; Schiava & Etse, 2006). For the localisation plastic discontinuities, it is actually shown that besides the importance of the localisation of bifurcation as presented by the above-cited works and the useful analysis of the slope movements considering diffuse strains like it is presented in this following, the mitigation of slope instability and its associated damages remains an essential question for the geotechnical engineer. Classical reinforcement techniques are in general expensive and not necessarily efficient when the slope failures have been observed to occur during or immediately after rainfall. Except the geotextile reinforcement with a drying function, for several authors the monitoring or warning systems offer viable alternatives (Brand, Premchitt, & Phillipson, 1984; Fabius & Bay, 2004; Keefer et al., 1987). Despite the slope-stability model development, the efficient numerical or analytical approaches connecting hydrologic and geotechnical processes are still not well-developed, particularly when the study goal is to improve practical solutions. Because the complexity of the problem, the existing models make many simplifying assumptions about the coupled nature of the failure process, the constitutive behaviour of the soil, the *in situ* hydraulic and environmental data as the rainfall intensity, the evaporation flux, and the *in situ* cyclic, hydraulic or mechanical stress conditions.

In this sense, the objectives of this paper are to use an efficient hydromechanical approach based on a numerical technique which has the capability to couple the solid deformation with fluid flow, and to study the effect of the kinetic infiltration on the initiation of deformations and then leads to the slope failure analyses. Unfortunately, the continuum nature of this model does not quantify the safety factor, unlike methods based on limit equilibrium approaches. Instead, the applied constitutive model in this study (BBM model), takes into account the suction effect as well as their dependence on degree of saturation. The BBM model predicts also the spatial and temporal variations of deformation, internal stresses and pore water pressure. To assess the potential for slope failure in the case of sandy soil, Borja and White (2010) used a criteria based on deformation bands as it was proposed by Rudnicki and Rice (1975), (Andrade & Borja, 2007). However, in the case of clayey soil, we use two criteria: the first is based on the volumetric deformation (particularly the volumetric plastic deformation component) and the second is based on the reduction of the yield function. As it is shown below, the reduction is characterised by the reduction of the apparent pre-consolidation stress and the cohesion. In fact, as in the elastoplastic model, the shear band concept is not yet introduced. The landslides analysis is conducted using the plastic deformation intensities (or the total displacement values). Also, we add in this analysis the reduction of the cohesion under humidification, via the apparent preconsolidation stress (as it is defined in the BBM model), as a parameter which can define the landslide zone (the zone where the cohesion filed is significantly reduced). This particular criterion is introduced in this paper as a new criterion.

In this paper, the elastoplastic BBM model has been applied to predict the local and shallow slope failure. This model can also be useful to give an explanation of the effect of the principal mechanical parameters which govern the behaviour of the soil. It is

important to note that via the BBM model, only the initiation of the slope movement can be described and not propagation. This idea is well discussed by Sanavia (2009). According to field observations and to field measured data, the failure modes are described and the numerical results are analysed. However, it must be noted that despite much effort to follow the site investigations and observations, much uncertainty remains particularly with respect to the geotechnical and hydrologic boundary conditions, the heterogeneity of geotechnical parameters. We emphasise that the few field instrumentations and the difficulty to access to a temporally continuum measurements, do not help to have an exhaustive data to assess whether the proposed model can predict the dependency of deformation and stresses on time and space coordinates. We only consider in the analysis reported in this paper, some topographical and inclinometer measurements. However, without exhaustive conclusion, it can be shown that this model can describe some realistic shallow failure modes and gives a tool to predict the initiation of the movements of slope. Also, the continuum deformation analyses should give us some recommendations for the use of practical solutions.

The paper starts with field investigations and soil properties that explore the relationship of soil nature to observed shallow slope failures, followed by sections describing different scenarios of rainfall intensity, rainfall duration and wetting–drying cycles. Inclinometer data collected during an occurred failure slope in March 2007 are used to partially assess whether the BBM model can successively integrate the hydro-mechanical parameters and still obtain a realistic description of the slope failure. The paper concludes with a discussion of future research directions.



## 2. Field observations

### *2.1. Failure cases*

As it is shown by Photos 1(a) and (b), shallow failures are triggered by the rainfall intensity as a prescribed forcing function. The damages are also localised due unlikely to local collapse arising from the water content increase. Also, the effective-mean-normal stress decreases further as a result of the loss of suction with increased degree of saturation. The slope is not so steep, on the order of 16 degrees. The depth of the shallow failure mechanism is much smaller than the minimum one which can be predicted by the limit equilibrium theory for a minimum factor of safety (Jamei, Guiras, Ben Hamouda, Hatira, & Olivella, 2008), thus making a continuum analyses approach appropriate for this problem. The collapse of the soil by the increase in the water

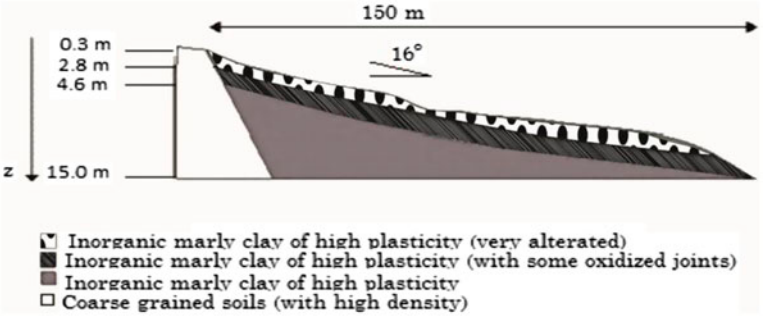


Figure 1. Topographic profile of the slope and stratified soil layers.

Table 1. Average rainfall intensity (in mm) per month for the 2000–2007 period.

| Year | 00/01 | 01/02 | 02/03 | 03/04 | 04/05 | 05/06 | 06/07 | Total | Average |
|---|---|---|---|---|---|---|---|---|---|
| SEPT | 106.9 | 58.8 | 23.9 | 93.7 | 45.7 | 24.8 | 39.0 | 392.8 | 56.11 |
| OCT | 104.2 | 12.0 | 20.8 | 45.9 | 14.9 | 17.7 | 47.0 | 262.5 | 37.5 |
| NOV | 17.4 | 21.1 | 140.0 | 34.7 | 154.5 | 32.4 | 39.6 | 439.7 | 62.8 |
| DEC | 42.2 | 40.0 | 83.8 | 187.3 | 108.6 | 86.4 | 121.8 | 670.1 | 95.7 |
| JAN | 133.8 | 27.7 | 229.0 | 91.1 | 51.9 | 212.1 | 12.3 | 757.9 | 108.3 |
| FEB | 29.8 | 23.5 | 112.3 | 18.6 | 117.1 | 84.4 | 39.7 | 425.4 | 60.77 |
| MAR | 22.4 | 90.5 | 15.9 | 72.8 | 43.2 | 25.4 | 147.7 | 417.9 | 59.7 |
| APR | 59.1 | 49.9 | 177.0 | 41.4 | 101.3 | 13.2 | 54.0 | 495.9 | 70.84 |
| MAY | 85.2 | 36.7 | 33.2 | 14.6 | 10.4 | 27.8 | 10.0 | 217.9 | 31.13 |
| JUNE | 5.4 | 10.5 | 12.9 | 119.4 | 16.0 | 2.6 | 32.6 | 199.4 | 28.4857 |
| JUL | 4.0 | 64.9 | .0 | .1 | 2.8 | .0 | .0 | 71.8 | 10.26 |
| AUG | .5 | 28.1 | .2 | 33.5 | 9.2 | 10.1 | 3.4 | 85.0 | 12.14 |
| Total | 610.9 | 463.7 | 849.0 | 753.1 | 675.6 | 536.9 | 547.1 | 4436.3 | 634 |

content is shown in Photo 1(b). The slope was failed locally as a large debris flow leading to shallow instability problems related to infrastructural works (Photo 1(a)). The following pictures (Photo 1) show some local failure events that occurred during 2006 and the damage produced to the road (Béja area).

Figure 1 describes the topographic profile of the slope and the nature of the soil, obtained from the field tests (test borings: drilling rig with mast in a down position). The instrumentation of the site included piezometers, meteorological sensors, moisture probes, inclinometers and topographic instruments. Continuous measurements from rainfall, discharge and total head (from selected piezometers) are available from 2000 to 2007.

### 2.2. *Rainfall data*

Rainfall data given in Table 1 show that during the period 2000 to 2007, the maximum rainfall intensity occurred often during November to February. The average value was 82 mm/month. In contrast, the average value of rainfall intensity was around 20 mm/month for the period between May and August, in which the evaporation was also more significant. The piezometric measurements during the year 2006 indicate that the ground water level or depth is between .5 m and 1.5 m. In the dry season, the soil is subjected to a high level of desiccation, leading to many cracks. Naturally the cracks induce a significant increase in compressibility, decrease in shear strength parameters and the increase in permeability. Evidently, this supposes the validity of such parameters' definition as a feature of porous media.

### 2.3. *Physical and Hydraulic soil properties*

As regards the physical properties of the clay soil, as shown in Table 2, across the depth of the soil, is clay, with different dry densities. The piezometric measurements during the year 2006 indicate that the ground water level or depth is between .5 and 1.5 m. In the dry season, the soil is submitted to a high desiccation level leading to many cracks and to an increase in its permeability.

Table 2. Physical properties of the clay soil (Ip: plasticity Index, $\omega_l$: Liquid limit).

| | | | % size distribution | | | Atterberg's limits | | Specific gravities (humid, dry and bulk), (gr/cm$^3$) | | | Porosity |
|---|---|---|---|---|---|---|---|---|---|---|---|
| Samples | Depth (m) | Water content $\omega$ (%) | %>0,42 (mm) | %<80 (μm) | %<2 (μm) | $\omega_l$ (%) | *Ip* (%) | $\gamma_h$ | $\gamma_d$ | $\gamma_s$ | $\phi$ |
| SC2EI1 | 1,4 ÷ 1,9 | 32 | – | 97 | 34 | 64 | 32 | 1.81 | 1.37 | 2.63 | .48 |
| SC1EI1 | 2,3 ÷ 2,8 | 27 | – | 97 | 21 | 51 | 25 | 1.88 | 1.48 | 2.65 | .44 |
| SC2EI2 | 3,4 ÷ 3,9 | 22 | 1 | 96 | 28 | 52 | 26 | 1.84 | 1.51 | 2.66 | .43 |
| SC2EI3 | 5,2 ÷ 5,7 | 29 | 1 | 94 | 20 | 56 | 28 | 1.87 | 1.45 | 2.65 | .45 |
| SC1EI2 | 14,5 ÷ 1,5 | 21 | 14 | 80 | 11 | 45 | 22 | 1.85 | 1.53 | 2.65 | .42 |

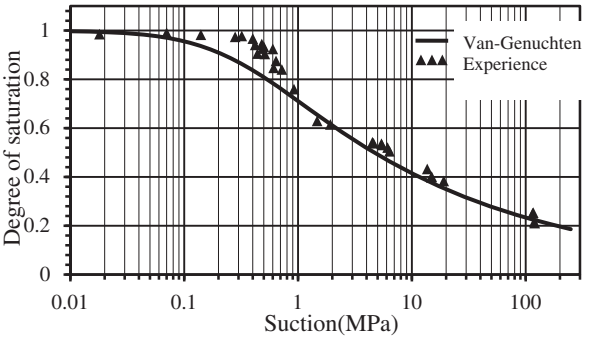


Figure 2. Water retention curve of the clay from Béja area.



Hydraulic properties of this marly clay (water retention curve, permeability function, intrinseque permeability) were investigated. The water retention curve was obtained across some conventional laboratory unsaturated tests (Romero, 2001). The laboratory conditions are the fixed temperature at $T = 20° \pm 2°$ and the fixed relative humidity at Hr = 50 ± 5%.

For the retention curve model, the Van Genuchten equation (empirical Model, Figure 2) was calibrated on this experimental data as following:

$$S_e = \frac{s_l - s_r}{s_s - s_r} = \left(1 + \left(\frac{u_a - u_w}{p}\right)^{\frac{1}{1-\lambda}}\right)^{-\lambda}; \quad \lambda = 0.2; \quad p = 0.1\text{MPa} \tag{1}$$

Some laboratory experimental tests have been performed on intact clayey specimens extracted from 1 m depth, such as oedometric tests on saturated specimens and undrained compression triaxial tests. The undrained cohesion is 80 kPa, (apparent cohesion), the undrained and effective friction angle are, respectively, 4° and 15° (apparent friction and drained friction angles). The pre-consolidation stress at saturation (suction $s = 0$) is 70 kPa and the conventional swelling stress is 50 kPa. The compressibility coefficient is .28 and the unloading (swelling) index is .07. Using the water retention curve, we obtain the air entry value around 100 kPa, which is defined as the suction at which the air permeates the material and the effective drying occurs (Peron, Hueckel Laloui, & Hu, 2009), and we assess the permeability at saturation as 10–7 m/s (Romero, Gens, & LIoret, 1999). The plasticity index (Table 2) shows the high plastic character of the soil, particularly for the surface layers. As it is mentioned below the higher the plasticity index, the higher the contractive behaviour and the desiccation process leading to crack pattern development.

## 3. Approach to model slope response to rainfall

The continuum slope model uses for the solid–water–air mixture has the following equations. Ignoring inertia forces, equilibrium equation is:

$$\nabla \cdot \sigma + \bar{\rho} g = 0; \quad \bar{\rho} = \phi^s \rho^s + \phi^w \rho^w \quad \text{with} \quad \phi^s + \phi^w = 1 - \phi^a \tag{2}$$

where $\phi^s, \phi^w$ and $\phi^a$ are, respectively, the solid, the water and the air volume fractions; $\rho^s$ and $\rho^w$ are, respectively, the solid and liquid mass densities. The air pressure is

assumed at the constant atmospheric value. Also all the following equations are written in isothermal conditions, which evidently leads to not considering the temperature gradient and limits the modelling of the evaporation (Gawin, Sanavia, & Schrefle, 1998).

If the water is assumed incompressible, the balance of water mass is (Borja, 2004):

$$\frac{\mathrm{d}\phi^w}{\mathrm{d}t} + \phi^w \nabla \cdot v + \nabla \cdot (\phi^w (v^w - v)) = \theta^w \tag{3}$$

where $v$ is the velocity of the solid matrix, $\theta^w$ is the rate of water with source exchange and $\mathrm{d}(\cdot)/\mathrm{d}t$ denotes the material time derivative following the solid motion.

The flow movement is described by the constitutive generalised Darcy's law, where

$$v - v^w = -\frac{k^{rw}}{\phi^w} \nabla \left( \frac{u_w}{\rho^w g} + z \right) \tag{4}$$

where $k^{rw}$ is the hydraulic tensor permeability of the unsaturated media and expressed as a product of a function of suction or degree of saturation (Romero et al., 1999) and the hydraulic conductivity tensor $K$ of the medium at saturation, $g$ is the gravity acceleration, and $z$ is the vertical coordinate.

We use the elastoplastic BBM model, proposed by Josa et al. (1990) for partially saturated soil. This model was formulated in terms of net stresses and suction and can be summarised by Figure 3(a), where a three-dimensional yield surface in ($p$, $q$, $s$) space is depicted. It is defined by two state surfaces explicitly based on two independent effective stress variables ($\sigma - u_a$) and the matrix suction ($u_a - u_w$). In triaxial conditions, the state surfaces are defined in the space of variables $p' = p - u_a$, $q$ and $s = u_a - u_w$, where $p$ is the invariant scalar which means the mean stress; $p = (\sigma_x + \sigma_y + \sigma_z)/3$ and $q = \left(\frac{1}{\sqrt{2}}\right)\sqrt{(\sigma_x - \sigma_y)^2 + (\sigma_z - \sigma_y)^2 + (\sigma_z - \sigma_x)^2 + 6\left(\tau_{xy}^2 + \tau_{zy}^2 + \tau_{xz}^2\right)}$ is the deviatoric stress. Under saturated conditions, the yield surface corresponds to the modified cam-clay (MCC) ellipse, and the size of the elastic domain increases as the suction increases (SI). The rate of increase, represented by the loading collapse (LC) curve (Figure 3(b)), is one of the fundamental characteristics of the model.

The BBM constitutive law becomes the classic MCC model when $s$ becomes zero (i.e. on reaching saturation). The set of equations of the BBM model is summarised as following (*Barcelona Basic Model (BBM)*; Josa et al., 1990). It is also useful to mention that the strong assumption of BBM model, is to consider the suction as a hardening parameter. This has been revised later by some authors (Laloui & Nuth, 2009; Nuth &

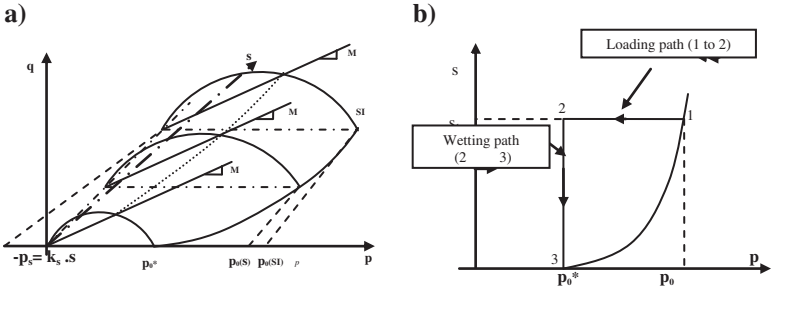


Figure 3. (a) Three-dimensional yield surface of Barcelona Basic model, (b) Yield surface in plane (s, p), mechanical and hydraulic paths.

Laloui, 2008). Also, with the BBM model, the yield surface evolves with the level of suction in a reversible manner.

yield surface (triaxial)
$$F(p,q,s) = q^2 - M^2(p + p_s(s))(p_o(s) - p) = 0 \quad (5)$$

Plastic potential (triaxial)
$$G(p,q,s) = q^2 - \alpha M^2(p + p_s(s))(p_o(s) - p) = 0 \quad (6)$$

Shear strength critical state parameter
$$M = \frac{6\sin\varphi\prime}{3 - \sin\varphi\prime} \quad (7)$$

Linear tensile strength
$$p_s(s) = k_s \quad (8)$$

LC curve
$$p_o(s) = p^c \left(\frac{p_o^*}{p^c}\right)^{\frac{\lambda(0)-\kappa}{\lambda(s)-\kappa}} \quad (9)$$

Isotropic elastoplastic volumetric deformation
$$\mathrm{d}\varepsilon_v = \frac{\lambda(s)}{1+e}\frac{\mathrm{d}p}{p} \quad (10)$$

Volumetric compressibility index
$$\lambda(s) = \lambda(0)\ [(1-r)\ \exp(-\beta s) + r] \quad (11)$$

Hardening law with plastic volumetric deformation
$$\mathrm{d}p_o^* = \frac{(1+e)p_o^*}{\lambda(0)-\kappa}\mathrm{d}\varepsilon_v^p \quad (12)$$

The parameters introduced in the models (Table 3) require some laboratory experimental tests. Some of them are measured as: $\varphi'$, $k_s$, $p_0^*$, $\lambda(0)$ and $\kappa$, where $\varphi'$ is the effective friction angle, $k_s$ is the material coefficient of the linear tensile strength evolution with suction $p_s(s)$, $p_0$ is the pre-consolidation stress at saturation, $\lambda(s)$ is a material parameter representing suction compressibility under constant mean stress and $\kappa$ is the slope of loading–reloading line for saturated state. The corresponded performed tests are, respectively, the consolidated undrained triaxial tests ($\varphi'$), the direct tensile tests with measured matric suction ($k_s$), (Trabelsi et al., 2012), and the oedometric tests under saturation ($p_0$, $\lambda(0)$ and $\kappa$). However, the parameters $r$, $\beta$ and $p^c$ are simply estimated, referring to results and empirical formula proposed in literature (Alonso, Vaunat, & Gens, 1999; Guiras-Skandaji, 1996; Josa et al., 1990; Sheng, Gens, Fredlund, & Sloan, 2008). Equation (9) is the so-called LC yield surface. Also $p$ is the reference mean

Table 3. Mechanical and hydraulic parameters for the constitute layers of slope.

| Parameters | $m_1$ | $m_2$ | $m_3$ | $m_4$ |
|---|---|---|---|---|
| $\Phi'$: friction angle | 15° | 15° | 10° | 30° |
| $M$: the slope of the critical state line (CSL) | .6 | .6 | .4 | 1.2 |
| $p_0$*: pre-consolidation stress at saturation (MPa) | .07 | .13 | .17 | 2 |
| $p^c$: reference stress (MPa) | .025 | .025 | .025 | .025 |
| $\kappa$: compressibility coefficient along elastic stress paths | .07 | .07 | .07 | .07 |
| $\lambda$ (0): compressibility coefficient for the saturated state along virgin loading | .28 | .28 | .28 | .05 |
| $k_s$: parameter of apparent cohesion | .1 | .1 | .1 | .1 |
| $K$: intrinsic permeability (m²) | $10^{-13}$ | $10^{-13}$ | $10^{-13}$ | $10^{-13}$ |
| $\phi$: initial porosity (%) | .5 | .5 | .5 | .4 |



stress. The $d\varepsilon_v$ and $d\varepsilon_v^p$ are, respectively, the total volumetric deformation and the plastic volumetric deformation.

The non-associated flow rule (α defines if it is associated or not. The associated flow rule is assumed, where $\alpha = 1$) which leads to the plastic strain calculation is given by:

$$d\varepsilon_{ij}^p = \chi \frac{\partial G}{\partial \sigma_{ij}} + \eta \frac{\partial G}{\partial s} \delta_{ij} \tag{13}$$

where $\chi$ and $\eta$ are positive plastic coefficients.

As this model is available in CODE_BRIGHT we have used this program to a series of analyses to gain understanding of the problem. These are presented in the next section together with the considered parameters.

The unsaturated permeability is given by the following equation:

$$K_{ns} = K_{sat} \sqrt{S_r} \left(1 - \left(1 - S_r^{1/\beta}\right)^{\beta}\right)^2 \tag{14}$$

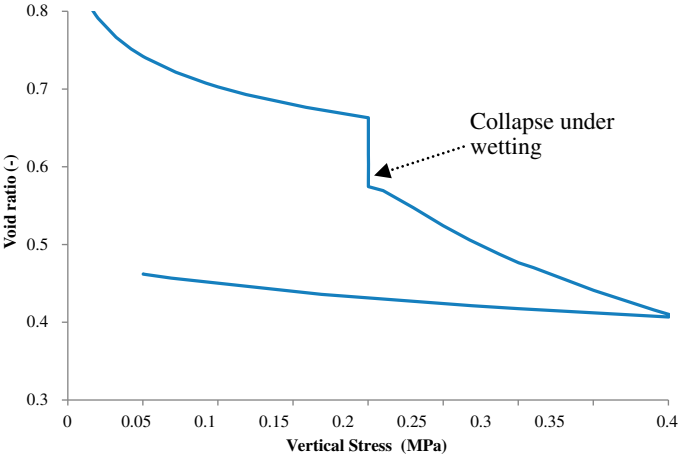


Figure 4. Simulation of an oedometer test in which collapse is induced at 200 kPa by wetting of the sample (initial suction is .2 MPa).

The $K_{sat}$ is the saturated permeability (m/s), $S_r$ is the degree of saturation and $\beta$ is a parameter depending on the soil.

To give an idea of the sensitivity of the BBM model with the mechanical parameters in Table 3, some basic laboratory tests are simulated numerically. Figure 4 shows the response of the unsaturated sample in oedometric test under vertical loading and wetting. As it is shown the collapse is produced under wetting and after a saturated sample is well compressed. The initial suction is .2 MPa and it is reduced to zero after wetting. In the other hand, the Figure 5 shows the response of the unsaturated soil under a deviatoric stresses and under a wetting at a given shear strain. The results show the capability of the model to predict the shear response under the hydro-mechanical coupled paths. The soft character of such material under saturation is well illustrated. The high compressibility and low strength of such material is well shown by the void ratio reduce (in oedometric test) and by deviatoric response after wetting stage. Actually, when the material is inundated the apparent cohesion is reduced to zero and the apparent pre-consolidation stress is reduced dramatically.

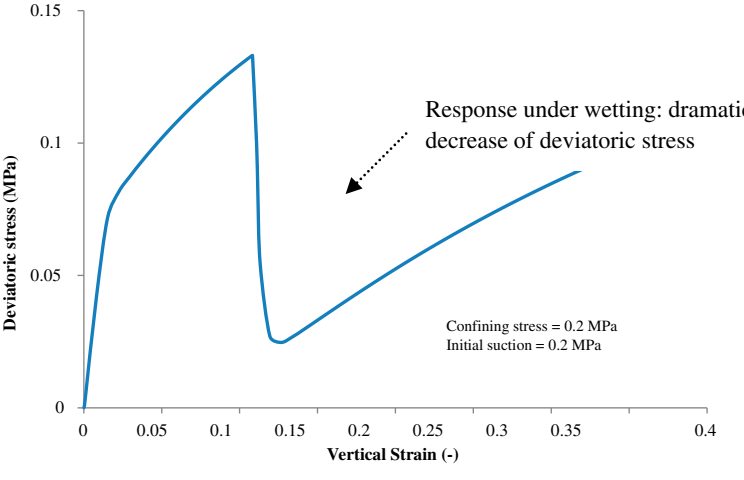


Figure 5. Simulation of a triaxial test with .2 MPa of confining stress and initial suction of .2 MPa. Wetting of the sample induces a lost of strength as pre-consolidation pressure change and the cohesion induced by suction vanishes.

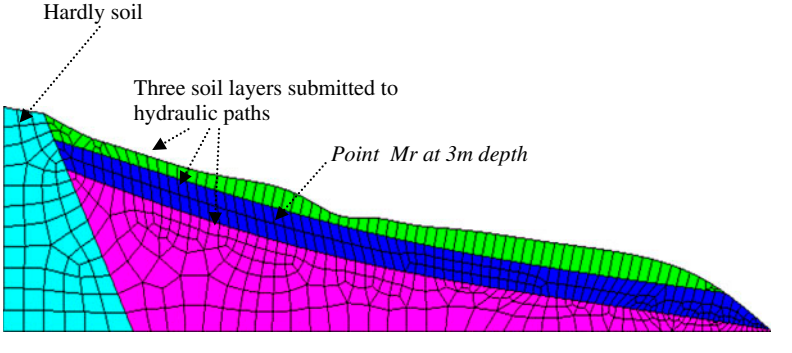


Figure 6. Mesh elements chosen for the simulations.

To apply the numerical analysis on the slope case studied here, the geometrical domain is exactly identified with the real dimensions. Figure 6 shows the mesh elements chosen for all the simulations presented in the following. The simulations are done according to the two following assumptions: small deformations and plane strains.

## 4. Analysis of the slope movements based on coupled hydromechanical numerical modelling

In order to provide useful answers to the field failures observed during the period between 2006 and 2007, numerical analysis was considered as a tool to understand the effect of several parameters. Such simulation is based on the rainfall data during wetting and drying seasons and on some field measurements. The movements of the slope which are strongly depended on both stress paths (mechanical and hydraulic stress paths) can be used as a measurement to evaluate the slope stability. As it is shown here after, two initial mechanical parameters of the soil (cohesion and apparent pre-consolidation stress) govern the movements of the slope according to the hydraulic path.

Three scenarios are considered in this study: the first corresponding to three rainfall sequences between November 2006 and February 2007, during 180 days. The second

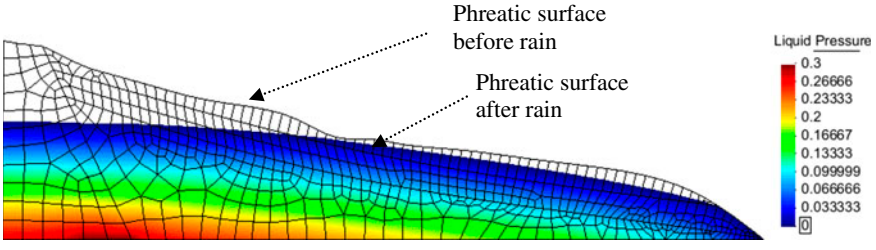


Figure 7. Evolution of the table water (positive water pressures) under rain.

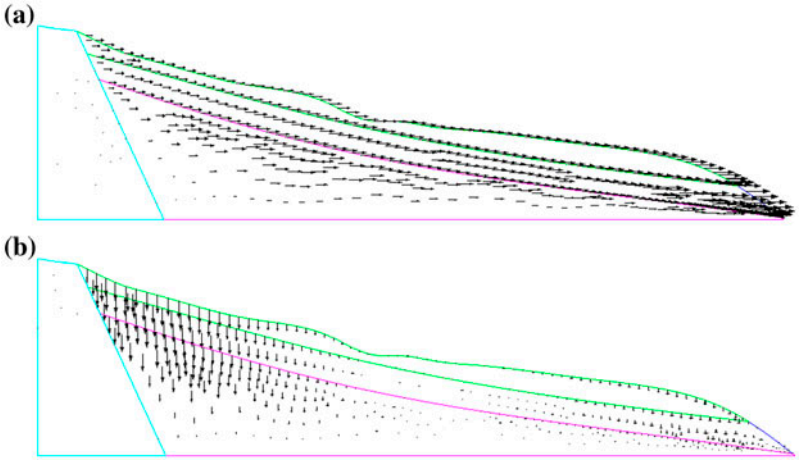


Figure 8. Horizontal (a) and vertical (b) displacement fields at the end of the infiltration (×25).

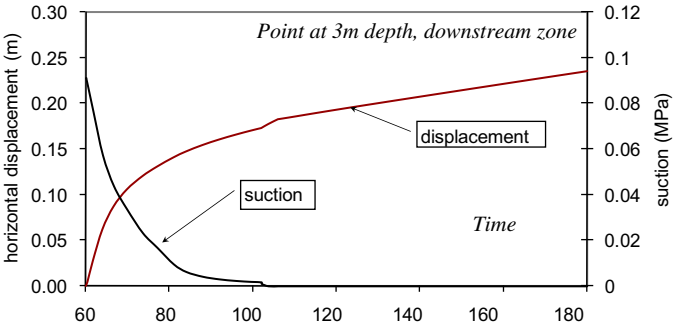


Figure 9. Horizontal displacement and suction evolutions during 120 days (upstream) [first scenario].

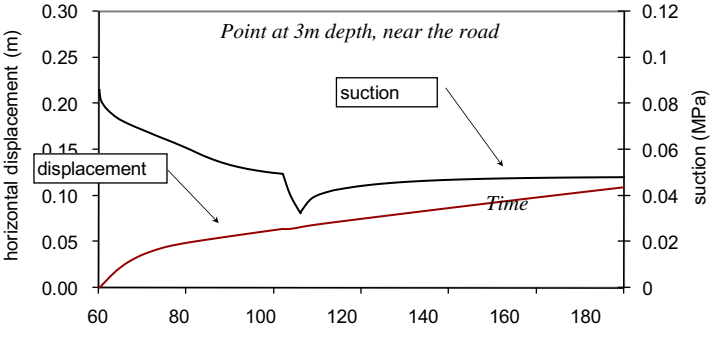


Figure 10. Horizontal displacement and suction evolutions during 120 days (near the road) [first scenario].

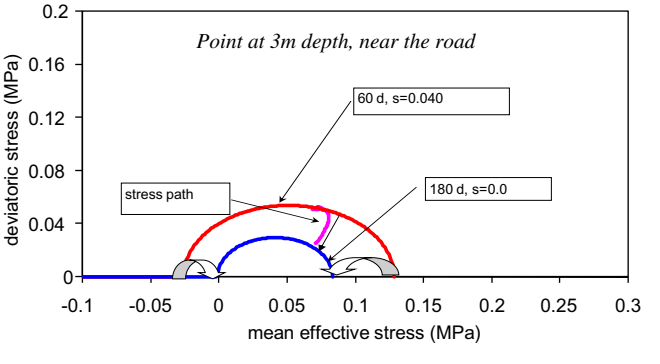


Figure 11. Yield surface evolution during the wetting path (near the road of the slope) [first scenario].

scenario takes into account the high and small levels of evaporation at 60 days which take place after a wetting process. Finally, in order to study the cycle effects (drying–wetting), one scenario which takes into account both cases: a wetting period added to a

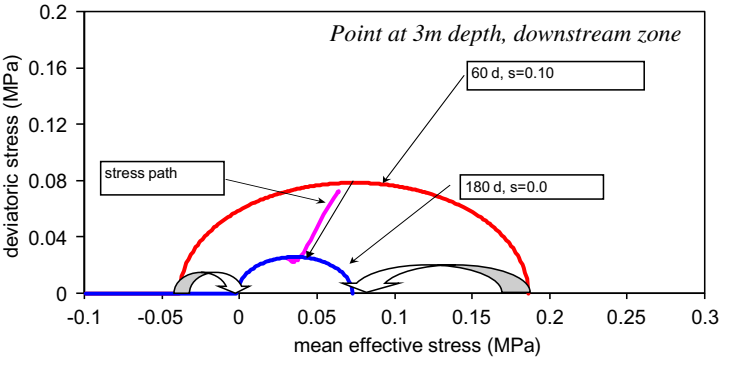


Figure 12. Yield surface evolution during the wetting path (downstream zone) [first scenario].

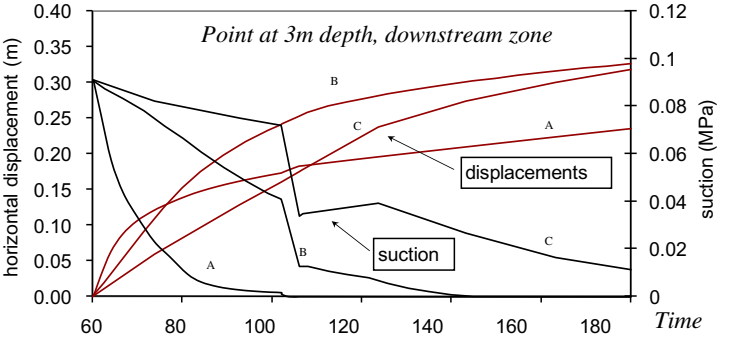


Figure 13. Horizontal displacement and suction evolutions for several saturated permeability (point Mr: near the road and for the high evaporation level) [second scenario].

long or a short period of drying (evaporation) is considered. For each case, the influence of the specific data on some mechanical parameters such as the cohesion and the apparent consolidated stress ($p^c$) are studied. A comparison between the numerical predicted results and the field measurements of the displacement in zones where the failures have been localised, using the few field experimental results performed by the inclinometer tests are given.

According to the geotechnical back-analysis based on the laboratory tests mentioned below in Section 3, for successive layers ($m_i$) are constituted by a soil which has the following properties. The relatively large intrinsic permeability corresponds to clay affected by cracks and heterogeneity (interlayer of permeable soils).

## 5. Moderate precipitation followed by a rainfall (first scenario)

For numerical simulations, we use in this section a realistic topographic profile of the studied slope as is it described above in Figure 1. Table 3 contains the corresponding properties required by the BBM model. The first scenario corresponds to a moderate precipitation during 102 days. A first period of 60 days is a period in which only boundary conditions of moderate evaporation were applied (we assume as a Dirichlet

boundary condition, the imposed suction value of 100 kPa). The boundary imposed condition is the fluid-flow (Neumann boundary condition). The rainfall is starting after this period during 42 days (from 60 to 102 day) with an average intensity of 2 mm/day. Then, a high value of 25 mm/day, corresponding to the short intensive rainfall (during 4 days, i.e. 106–110 day) was applied. For these simulations, precipitation is described by the fluid-flow fixed at the corresponding value of each scenario. However, the evaporation is simulated by fixing a suction value or a negative fluid-flow at the slope surface.

Figure 7 shows the position of the phreatic surface before and after rain. Only the positive pressures are shown to indicate the evolution of the saturated zones. Modelling the slope movement requires the initial conditions (hydraulic conditions). In this particular case, to compare the numerical displacement field with the measured one, the initial state corresponds to the phreatic surface determined by the piezometer measurements before strain. In the unsaturated zone, the suction is considered constant, corresponding to the effective cohesion measured in laboratory. The relation between the cohesion and suction is described by the Equation (8), via the preconsolidation stress. On the other hand, for the given numerical tests used for the analysis, the suction is constant in the unsaturated zone corresponding to a given value as it is indicated for each corresponding figure.

Figure 8 also shows the horizontal and vertical fields of displacement, which indicate that the vertical ones correspond to the consolidation under wetting, and the horizontal ones are more importantly near and in the downstream of the road and are motivated by the reduction of strength.

Figure 8 shows displacement field trend which indicates that the horizontal component of movement is more important in the downstream side of the slope. In the upstream side, the vertical displacement values corresponding to collapse is also significant. The maximum displacement value was calculated around 25 cm (Figure 9) and it can be observed that the increase in the rain intensity did not produce a major change in the response (at 106 day) as the soil was already wet due to the previous long-term low intensity rainfall. Figure 10 shows a similar response rather at a point near the road.

In order to understand the deformation processes especially when dealing with plastic strain, in this case induced by changes in suction, it is essential to look at the stress suction paths. Figure 11 shows both decrease in the cohesion and the apparent pre-consolidation stress when the suction decreases (from 60 day to 180 day, suction decreased from .1 to 0 MPa). The reduction of the yield surface reduces the strength

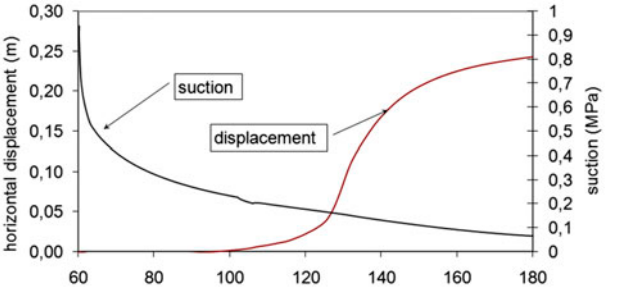


Figure 14. Horizontal displacement and suction evolutions during 120 days (near the road and for the high evaporation level) [second scenario].

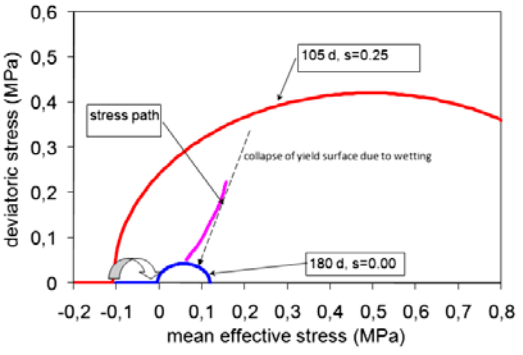


Figure 15. Yield surface evolution during the wetting path (near the road of the slope and for the high evaporation level) [second scenario].

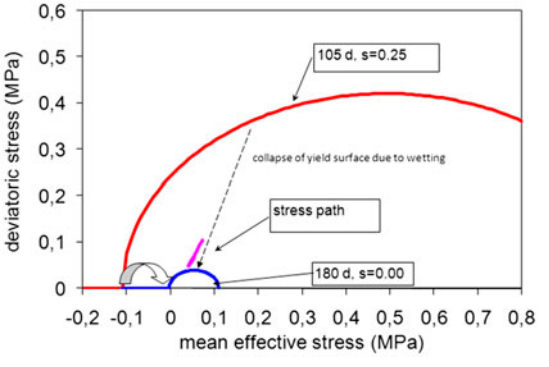


Figure 16. Yield surface evolution during the wetting path (downstream zone and for the high evaporation level) [second scenario].

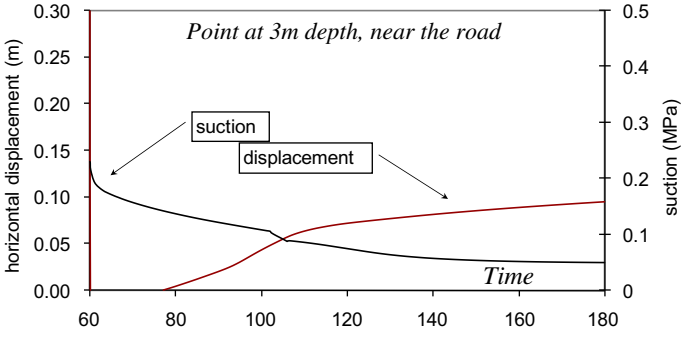


Figure 17. Horizontal displacement and suction evolutions during 120 days (near the road and for the small evaporation level) [second scenario].

and causes collapse deformation (Figures 11 and 12). It was mentioned otherwise (Alonso & Romero, 2003) that collapse under wetting leads to a serious problem of stability of soil even though it is a sandy soil. In the case of this considered scenario,

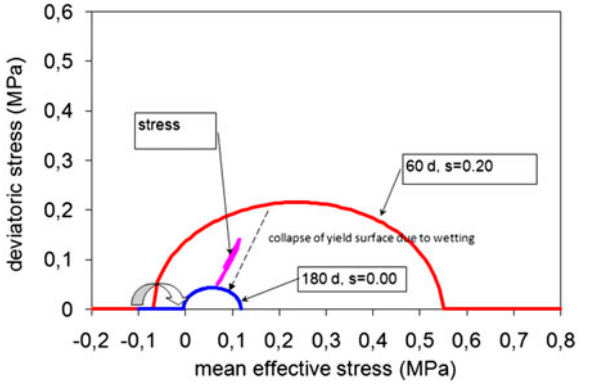


Figure 18. Yield surface evolution during the wetting path (near the road of the slope and for the small evaporation level) [second scenario].

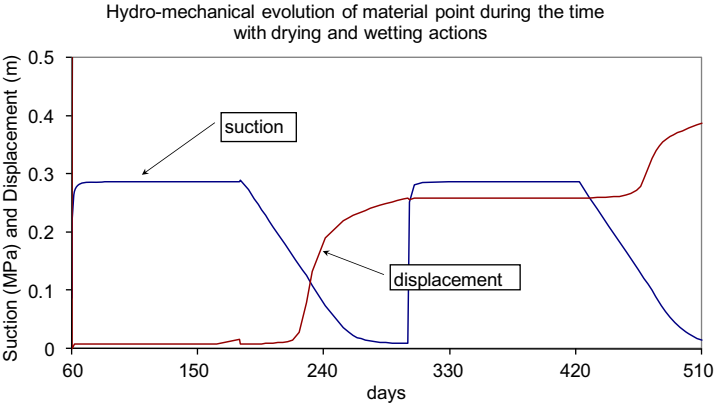


Figure 19. Suction and horizontal displacement evolutions against the time during 450 days and for the two hydraulic cycles [third scenario] (point $M_1$ with coordinates (7.77, 410.960)).

the plastic deformations are moderate. Under the hydraulic boundary conditions in this case, the larger displacements are located in the downstream of the slope and not near the road (Figure 10).

Figure 13 shows the effect of permeability. The values considered are A: $5 \times 10^{-13}$ m$^2$, B: $5 \times 10^{-14}$ m$^2$ and C: $5 \times 10^{-15}$ m$^2$ corresponding to increasing homogeneity and intactness. For lower permeability the wetting is slower and also it delays the development of movements. The final displacement values are lower for higher permeability which may be due to stress paths going inside the yield surface as the soil saturates. The permeability evolution in the *in situ* conditions may be related to porosity evolution, which occurs specially in the dry season in the upper layers. However, whereas the importance of permeability on the hydrologic and mechanical aspects has been elucidated from previous simulations (Borja, 2010; Ebel et al., 2007; Montgomery, Dietrich, Torres, Anderson, & Loague, 1997), its evolution with the desiccation effects, is still poorly understood and it is yet an open question. Evidently, if the desiccation

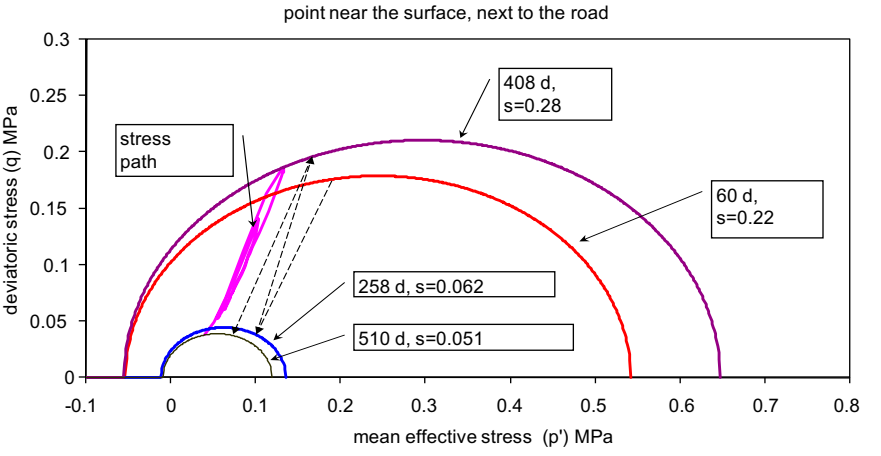


Figure 20. Yield surface evolution under the hydraulic cycles (stress path for material point at the slope's surface and next to the road) [third scenario].

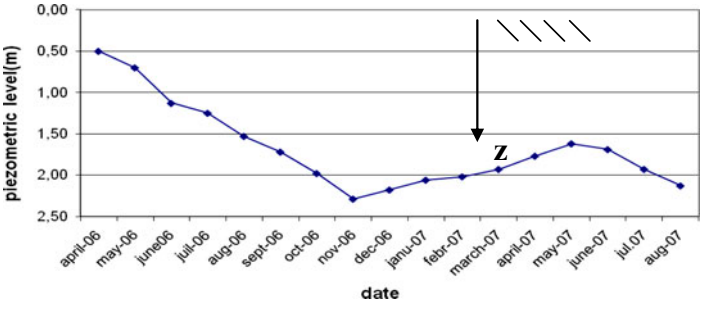


Figure 21. The groundwater level measured during the years 2006 and 2007.

process produces largely opened cracks (strong discontinuities), the definition of the permeability in the sense of porous media mechanics, losses its sense.

### *5.1. Period of high and low suction followed by rainfall (second scenario)*

In this section, we show the effect of the initial evaporation conditions on the slope movements and on the localized failure zones. Hence, during a period of 60 days, a drying path was applied across a boundary condition via the imposition of the suction (Dirichlet boundary condition), corresponding, respectively, to different cases: high and small evaporation levels (respectively, $s_i$ = 1 MPa, and $s_i$ = .2 MPa).

In this section, the choice of these suction values is arbitrary; given that the goal is to study the effect of the evaporation level which is assumed to be straightly related to suction level. In fact, in the case of initial high evaporation level, the unsaturated zone in which the capillarity suction has been developed increases, hence the cohesion and the apparent pre-consolidation stress increases. Consequently, under the wetting path, the clayey soil

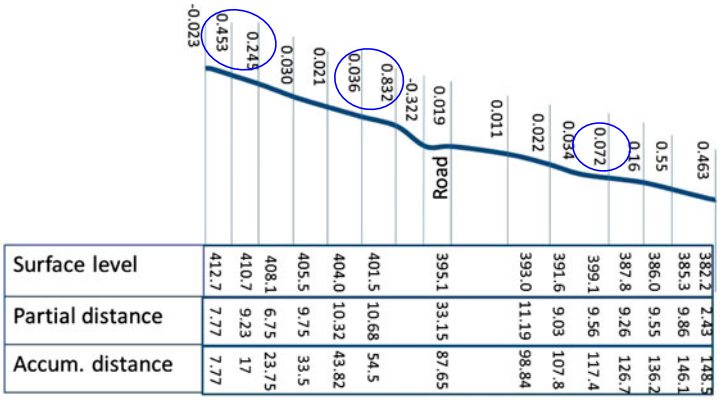


Figure 22. Total displacement measured by the inclinometer test at the slope surface (the measures was kept between from 11/2006 to 03/2007).

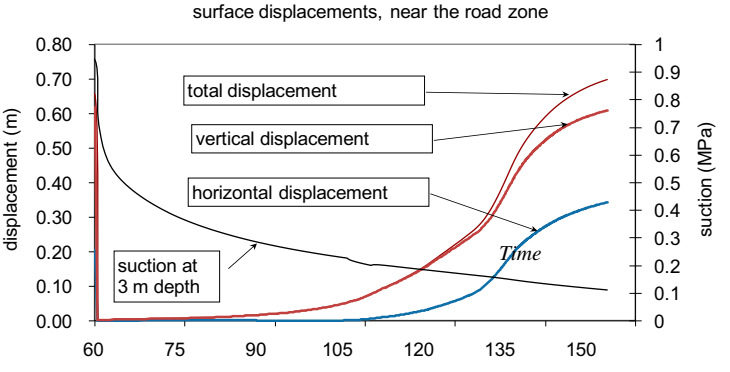


Figure 23. Displacements and suction evolutions against the time during 90 days at the point $M_3$ at the upstream of the road.

collapsed and both parameters (cohesion and apparent pre-consolidation stress) dramatically decreased (Figures 15 and 16). The horizontal displacement value near the road was found around 25 cm (Figure 14), but it was higher in the downstream zone (around of 45 cm). It can be shown that at the inception of the collapse mechanism due to wetting (increase in the plastic volumetric deformation), the failure is locally more focused, particularly in the downstream of the slope. In the zone near the road, the collapse also leads to a shallow failure. In the opposite, when the evaporation is not so higher, under the same conditions of wetting (duration and intensity) the failures are not so occurred.

Note that the intermediate (105 days) and the final (180 days) yield surfaces are represented (Figure 15).

When the evaporation is smaller (suction of .2 MPa) and the same conditions of wetting applied (duration and intensity), the movements were much smaller (Figure 17). The explanation is that when the initial evaporation is smaller the same conditions of wetting do not produce the same effects of decrease in cohesion and apparent pre-consolidation stress, and therefore the slope movements were smaller (Figures 17 and 18).


Photo 1. (a) Shallow failures causing damages in the road, (b) Collapse of the clay soil during a period of wetting season [a] (date: 16/03/2006), Local slope failure after the first rainfall episode [b] (date: 20/12/2006).


Photo 2. Local failure near the road (this photo was taken at 15 March 2007).

Therefore, a short-duration intensive rainfall, especially after a high drying period, tends to accelerate slope movements and leads eventually to failure (Figures 14 and 16). As it is mentioned above, the localized zone is identified by the total displacement field values or by the cohesion field. In order to compare the numerical and field measurements, the total displacement field criterion is rather considered.

From the numerical study, it has been shown that the higher the suction at the onset of rainfall, the higher the irreversible displacements. Then, if we take into account the irreversible horizontal displacement component as an evaluation criterion of the sliding, resulting from the loss of the cohesion and pre-consolidation stress, we can extrapolate the criterion to potential failure and collapse of the soil.

### 5.2. *Evaporation and rainfall cycles (third scenario)*

This case is intended to investigate the effect of environmental cycles of drying and wetting due to annual seasonal effects. An initial suction of $s_i$ = .33 MPa was applied on the surface and kept constant during the period between 60 days and 180 days. It corresponds to the first drying period. Then during a period of 78 days (between 180 days and 258 days) the humidification path was applied by means of rain with small intensity. From numerical point of view, the rain is described via its intensity which is transformed to a fluid-flow expressed by mm/day by unit surface ($m^2$). As a consequence, the suction decreases from .285 to 0.062 MPa at the point represented in Figure 19 (near the road). A second cycle was applied afterwards. In the first cycle, the displacement increases dramatically during the wetting path with a calculated increment of .26 m, while in the second cycle, the increment is only .12 m (Figure 19). So it is clear that the displacement increment during the first wetting is roughly double that of what occurred during the second wetting. This is a consequence of hardening developed by collapse under a plastic deformation initiation (Figure 20). Still, the yield surface evolution is more reduced for the second wetting cycle, for the apparent pre-consolidation stress and for cohesion.

## 6. Incorporation of the seasonal precipitation and evaluation of calculated and measured movements

During the period April 2006 to August 2007, the underground water level was measured using the piezometer. Figure 21 shows the variation of the water level which is significant between the wet and the dry seasons (depth varies from .67 to 2.13 m).

It seems that the difference of this model and the case presented in Section 4.1 is the history of imposed precipitation. Finally, Figure 22 shows some measurements using inclinometer and topographic relative total displacements that were recorded during a campaign that was performed until the end of March 2007 and during the wet season. In Figure 22, the inclinometers positions are indicated and one set of measurements recorded during the failure of 30 March 2007 is given. The given displacements values corresponding to inclinometers and topographic measurements are taken in the top of the layer $m_1$. As the resulting slope movement was followed by the combined measurements (topographic for the total displacement and inclinometer for the horizontal displacement, the data presented in Figure 23 results from a treatment of the measurement information).

An attempt to reproduce the field measurement data was done by modelling the period from December to March (180 days) which was subdivided into two sequences: an evaporation period of 60 days corresponds to an equilibrium suction of 1 MPa; then an infiltration flux data corresponding to three intervals of 42 days, 4 days and 74 days, respectively, ($2 \times 10^{-5}$ kg/s/$m^2$, $3 \times 10^{-4}$ kg/s/$m^2$ and $10^{-5}$ kg/s/$m^2$: Neumann boundary conditions), (see Table 4).

Table 4. Hydraulic boundary conditions.

| Period (days) | 0–60 | 60–102 | 102–106 | 106–180 |
|---|---|---|---|---|
| Boundary condition | Dirichlet condition: Suction fixed at 1MPa | Neumann condition: Flux is fixed at $+2 \times 10^{-5}$ kg/s/m$^2$ | Neumann condition: Flux is fixed at $+3 \times 10^{-4}$ kg/s/m$^2$ | Neumann condition: Flux is fixed at $+10^{-5}$ kg/s/m$^2$ |
| Hydraulic path | drying | wetting | wetting | wetting |

The calculated displacement shown in Figure 23 (the results corresponded to point $M_3$(10.68, 399.398)), is in the same order of magnitude as that as in the field, (Figure 22). It was observed in the field that the soil was fully saturated near the surface at the moment of maximum movements.

Photo 2 shows the local failure that took place near the road which was the zone with more tendency to instability due to the shape of the surface and the larger infiltration. The range of total displacement predicted by the model is in agreement with the failure observed near the road. Despite the interesting quality of this qualitative comparison between numerical and field experimental results, it appears that not knowing the field boundary conditions and the effect of fractured layers (i.e. crack pattern and depth of cracks), it is unlikely to reproduce the exact field failures.



## 7. Conclusion

Based on the field observations, field measurements and numerical calculations, the following conclusions can be given:

The inclinometer measurements and the field observations (many photos have been taken during the period of landslides) showed the locally and shallow failures along the slope. At the same time, these failures were more frequent after long dry seasons and under high rainfall intensity.

Using the rainfall events data, the underground water level (piezometric data) and the geotechnical data (water retention and grain distribution curves, compressibility coefficients, cohesion and friction angle values), simulations based on poro-elastoplastic model for unsaturated soils were performed. Unfortunately, knowing the exact field boundary conditions remains difficult. For this reason, some assumptions of boundary conditions date were given.

The collapse observed on the surface of the slope in terms of the increase in volumetric strain (at a depth below 3 m) was related to the evolution of both variables: suction and apparent pre-consolidation stress. A high decrease in soil suctions takes place due to rain. This induces a significant decrease in apparent pre-consolidation stress and plastic deformations. When the soil was subjected to wetting/drying cycles during a total period of 510 days or to high rainfall intensity in a long period, the movements were more significant.

It appears that the apparent pre-consolidation stress controls the strength. In fact, under the same variation of suction, the decrease in the yield surface domain depends also on the initial pre-consolidation stress value: the higher the value, the higher the relative decrease in the yield surface domain will be.

The BBM elastoplastic model is appropriate to give the prediction of the shallow and local failures which take place under high soil suction reduction. The key points in the model are the apparent pre-consolidation stress evolution and the consideration of the rainfall data. Therefore, the BBM elastoplastic model should help in understanding practical behavioural features – for example, using the geotextile or coarse materials for drainage – by leading to optimise the kind of material and positions of drains. The two kinds of the solutions offer a channel-flow by drainage and maintain the seepage infiltration on the slope surface (case of coarse materials) or across the geotextile sheet. Both techniques dissipate pore water pressure and avoid the dramatical decrease in suction and as a consequence avoid the decrease in cohesion and apparent pre-consolidation pressure.

As it was demonstrated elsewhere (Jamei et al., 2008), the equilibrium approach is not sufficient for the prediction of the actual (field) shallow movements and failure and cannot incorporate easily the collapse phenomena.

The effect of the initiation of the collapse of the clay in the upstream of the slope (by the increase in vertical displacement and then the volumetric deformation) has been shown and it can be the origin of the increase in failure displacement. The prediction of the vertical movement via the poro-elastoplastic model improved these field observations.

On the surface of the slope, a crack pattern has been well observed (Jamei et al., 2008). This phenomenon could lead to an increase in permeability and enhance shallow slope instability (Istanbulluoglu, Bras, & Flores-Cervantes, 2005). Taking into account the cracking and the subsequent permeability variation should be a future challenge of this research.

In order to improve the validation of the performance of the proposed analysis approach, a further complementary field and laboratory measurements (water content and suction along depth, suction using tensiometers, thermal conductivity, suction sensors, moisture probes, inclinometers, evaporimeter) should be performed.

From an engineering point of view, the reinforcement solution or the performance technique to use for the slope stability may be the challenge of this study. From our point of view, only with an extensive analysis of this slope instability problem, we can discuss the performance of practical technical solutions as the geotextile reinforcement or the channel coarse grains solution in order to dissipate the interstitial pressure and to reduce the effect of the hydraulic forces action.

## Acknowledgements

The authors would like to acknowledge Béja Regional Administration of the Ministry of Equipment (Tunisia), for their participation in the field tests and for their support of this research project.

## References

Alonso, E. E., & Lioret, A. (1983). *Evolution in time of the reliability of slopes in partially saturated soils*. Fourth International Conference on Applications of Statistics and Probability in Soil and S structural Engineering, Italy.

Alonso, E. E., & Romero, E. (2003). Collapse behaviour of sand. In *Proceeding Asian Conference on Unsaturated Soils* (pp. 325–333). Osaka, Japan.

Alonso, E. E., Vaunat, J., & Gens, A. (1999). Modelling the mechanical behaviour of expansive clays. *Engineering Geology, 54*, 173–183.

Andrade, J. E., & Borja, R. I. (2007). Modeling deformation banding in dense and loose fluid-saturated sands. *Finite Elements in Analysis and Design, 43*, 361–383.

Au, S. W. C. (1998). Rain-induced slope instability in Hong Kong. *Engineering Geology, 51*, 1–36.

Borja, R. I. (2004). Cam-Clay plasticity. Part V: A mathematical framework for three-phase deformation and strain localization analyses of partially saturated porous media. *Computer Methods in Applied Mechanics and Engineering, 193*, 5301–5338.

Borja, R. I. (2010). Conservation laws for coupled hydro-mechanical processes in unsaturated porous media: Theory and implementation. In L. Laloui (Ed.), *Mechanics of Unsaturated Geomaterials* (pp. 185–208). Lausanne: Wiley.

Borja, R. I., & White, J. A. (2010). Continuum deformation and stability analyses of a steep hillside slope under rainfall infiltration. *Acta Geotechnica, 5*, 1–14.

Brand E. W., Premchitt J., & Phillipson H. B. (1984). Relationship between rainfall and landslides in Hong Kong. In *Proceedings, 4th International Symposium on Landslides* (pp. 377–384). Toronto.

Buscarnera, G., & Prisco, C. (2012). Discussing the definition of the second-order work for unsaturated soils. *International Journal for Numerical and Analytical Methods in Geomechanics, 36*, 36–49.

Chapuis, R. P., & Chenaf, D., Bussière, B., Aubertin, M., & Crespo, R. (2001). A user's approach to assess numerical codes for saturated and unsaturated seepage conditions. *Canadian Geotechnical Journal, 38*, 1113–1126.

Dai, F. C., Lee, C. F., & Sijing, W. (1999). Analysis of rainstorm induced slide-debris flows on natural terrain of Lantau Island, Hong Kong'. *Engineering Geology, 51*, 279–290.

Ebel, B. A., Loague, K., VanderKwaak, J. E., Dietrich, W. E., Montgomery, D. R., Torres, R., & Anderson, S. P. (2007). Near-surface hydrologic response for a steep, unchanneled catchment near Coos Bay, Oregon: 2. *Physics-based simulations. American Journal of Science, 307*, 709–748.

Fabius, K., & Bay, T. (2004). Slope hazard management with the cautionary zone approach: A case history. *57th Canadian Geotechnical Conference*. Quebec City, Canada.

Fernandez Merodo, J. A., Pastor, M., Mira, P., Tonni, L., Herreros, M. I., Gonzalez, E., & Tamagnini, R. (2004). Modelling of diffuse failure mechanisms of catastrophic landslides. *Computer Methods in Applied Mechanics and Engineering, 193*, 2911–2939.

Gawin, D., Sanavia, L., & Schrefler, B. A. (1998). Cavitation modelling in saturated geomaterials with application to dynamic strain localization. *International Journal for Numerical Methods in Fluids, 27*, 109–125.

Gong, B. W., Bao, C. G., Ng, C. G., Fredlund, D. G., & Zhan, L. T. (2003). Performance of an unsaturated expansive soil slope subjected to artificial rainfall infiltration. *Géotechnique, 53* (2), 143–157.

Guiras-Skandaji, H. (1996). *Déformabilité des sols argileux non saturés: étude expérimentale et application à la modélisation* [Unsaturated clay soil deformability: Experimental study and modelling application] (Thèse de Doctorat Institut Polytechnique de Lorraine). Ecole Supérieure de Géologie de Nancy, Juin.

Herrores, M., FernÁndez Merodo, J. A., Quecedo, M., Mira, P., Pastor, M., & GonzÁlez, E. (2002). Modelling tailings dams and mine waste dumps failures. *Géotechnique, 52*, 579–591.

Istanbulluoglu, E., Bras, R. L., & Flores-Cervantes, H. (2005). Implications of bank failures and fluvial erosion for gully developement: Field observations and modeling. *Journal of Geophysical Research, 110*, 1–21.

Jamei, M., Guiras, H., Ben Hamouda, K., Hatira, M., & Olivella, S. (2008). A study of the slope stability in unsaturated marly clay soil. *Studia Geotechnica et Mechanica, XXX*, 95–106.

Josa, A., Alonso, E. E., & Gens, A. (1990). A constitutive model for partially saturated soils. *Géotechnique, 40*, 405–430.

Keefer, D. K., Wilson, R. K., Mark, R. K., Brabb, E. E., Brown, W. M., Ellen, S. D., … Zatkin, R. S. (1987). Real-time landslide warning during heavy rainfall. *Science, 238*, 921–925.

Laloui, L., & Nuth, M. (2009). On the use of the generalized effective stress in the constitutive modeling of unsaturated soil. *Computer and Geotechnics, 36*, 20–23.

Lim, T. T., Rahardjo, H., Chang, M. F., & Fredlund, D. G. (1996). Effect of rainfall on matric suctions in a residual soil slope. *Canadian Geotechnical Journal, 33*, 618–628.

Montgomery, D. R., Dietrich, W. E., Torres, R., Anderson, S. P., & Loague, K. (1997). Hydrological response of a steep, uneled valley to natural and applied rainfall. *Water Resources, 33*, 91–109.

Nicot, F., Darve, F., & Dat Vu Khoa, H. D. V. (2007). Bifurcation and second-order work in geomaterials. *International Journal for Numerical and Analytical Methods in Geomechanics, 31*, 1007–1032.

Nuth, M., & Laloui, L. (2008). Effective stress concept in unsaturated soil: Clarification and validation of the unified framework. *International Journal for Numerical and Analytical Methods in Geomechanics, 113*, 771–801.

Orense Rolando, P., Suguru, S., Kengo, M., & Ikuo, T. (2004). Instrumented model slope failure due to water seepage. *Journal of Natural Disaster Science, 26*, 15–26.

Pastor, M., Quecedo, M., Gonzalez, E., Herreros, M. I., Fernandez Merodo, J. A., & Mira, P. (2004). Numerical modelling of the propagation of fast landslides using the finite element method. *International Journal for Numerical Methods in Engineering, 59*, 755–794.

Pastor, M., Blanc, T., Stickle, M. Martin, Dutto P., Mira P., Fernández Merodo J. A., Sancho S., Benítez A. S. (2013), March 14-16. Mathematical, constitutive and numerical modeling of catastrophic landslides and related phenomena. In *Proceedings of the First International Conference on Landslides' Risk* (pp. 3–30), Tabarka (Tunisia), 14–15 and 16 March 2013.

Peron, H., Hueckel, T., Laloui, L., & Hu, L. B. (2009). Fundamentals of desiccation cracking of fine-grained soils: Experimental characterisation and mechanisms identification. *Canadian Geotechnical Journal, 46*, 1177–1201.

Rees, S. W., & Thomas, H. R. (1994). Seasonal ground movement in unsaturated clay: An examination of field behaviour. *Géotechnique, 44*, 353–358.

Romero, E. (2001). Controlled-suction techniques. In W. Y. Y. Gehling & F. Schnaid (Eds.), *Proc. 48 Simpoesio Brasileiro de Solos Naô Saturados, Porto Alegre. Associacaõ Brasileira de Mecanica dos Solos e Engenharia Geote'cnica ABMS* (pp. 535–542). Porto Alegre, Brasil.

Romero, E., Gens, A., & LIoret, A. (1999). Water permeability, water retention and microstructure of unsaturated compacted Boom clay. *Engineering Geology, 54*, 117–127.

Rudnicki, J. W., & Rice, J. R. (1975). Conditions for the localization of deformation in pressure-sensitive dilatant materials. *Journal of the Mechanics and Physics of Solids, 23*, 371–394.

Sanavia L. (2009). Numerical modelling of a slope stability test by means of porous media mechanics. *Engineering Computations, 26*, 245–266.

Schiava, R., & Etse, G. (2006, April 6). Constitutive modeling and discontinuous bifurcation assessment in unsaturated soils. *Journal of Applied Mechanics, 73*, 1039–1044 (6 pages) doi:10.1115/1.2202349

Sheng, D., Gens, A., Fredlund, D. G., & Sloan, S. W. (2008). Unsaturated soils: From constitutive modelling to numerical algorithms. *Computers and Geotechnics, 35*, 810–824.

Smith, P. G. C. (2003). Numerical analysis of infiltration into partially saturated soil slopes (A thesis submitted to the University of London).

Tamagnini R., & Pastor M. (2004). A thermodynamically based model for unsaturated soils: A new framework for generalized plasticity. In *Proceedings 2nd International Workshop on Unsaturated Soils*, Capr.

Trabelsi, H., Jamei, M., Guiras, H., Zenzri, H., Romero, E., & Olivella, S. (2012). Some investigations about the tensile strength and the desiccation process of unsaturated clay. In F. Brémand (Ed.), *ICEM 14 – 14th International Conference on Experimental Mechanics, Poitiers*, France; EPJ Web of Conferences (pp. 1–8). Vol. 6, id.12005.

Zhang, L. L., Zhang, L. M., & Tang, W. H. (2005). Rainfall-induced slope failure considering variability of soil properties. *Géotechnique, 55*, 183–188.